https://helda.helsinki.fi

Measurement of the relative yields of psi(2S) to psi(1S) mesons produced at forward and backward rapidity in p plus p, p plus Al, p + Au, and He-3+Au collisions at root S-NN=200 GeV

Adare, A.

2017-03-09

Measurement of the relative yields of $\psi(2S)$ to $\psi(1S)$ mesons produced at forward and backward rapidity in $p + p$, $p +$ Al, $p +$ Au, and ^{3}He +Au collisions at $\sqrt{s_{NN}} = 200$ GeV

A. Adare,[13] C. Aidala,[40] N. N. Ajitanand,[56] Y. Akiba,[51,52,*] M. Alfred,[23] V. Andrieux,[40] K. Aoki,[31,51] N. Apadula,[28,57]
H. Asano,[34,51] C. Ayuso,[40] B. Azmoun,[7] V. Babintsev,[24] M. Bai,[6] N. S. Bandara,[39] B. Bannier,[57] K. N. Barish,[8] S. Bathe,[5,52]
A. Bazilevsky,[7] M. Beaumier,[8] S. Beckman,[13] R. Belmont,[13,40] A. Berdnikov,[54] Y. Berdnikov,[54] D. S. Blau,[33] M. Boer,[36]
J. S. Bok,[45] E. K. Bownes,[41] K. Boyle,[52] M. L. Brooks,[36] J. Bryslawskyj,[5,8] V. Bumazhnov,[24] C. Butler,[21] S. Campbell,[14,28]
V. Canoa Roman,[57] R. Cervantes,[57] C.-H. Chen,[52] C. Y. Chi,[14] M. Chiu,[7] I. J. Choi,[25] J. B. Choi,[10,†] T. Chujo,[60] Z. Citron,[62]
M. Connors,[21,52] N. Cronin,[41,57] M. Csanád,[17] T. Csörgő,[18,63] T. W. Danley,[46] A. Datta,[44] M. S. Daugherity,[1] G. David,[7]
K. DeBlasio,[44] K. Dehmelt,[57] A. Denisov,[24] A. Deshpande,[52,57] E. J. Desmond,[7] A. Dion,[57] P. B. Diss,[38] D. Dixit,[57] J. H. Do,[64]
A. Drees,[57] K. A. Drees,[6] M. Dumancic,[62] J. M. Durham,[36] A. Durum,[24] J. P. Dusing,[41] T. Elder,[18,21] A. Enokizono,[51,53]
H. En'yo,[51] S. Esumi,[60] B. Fadem,[41] W. Fan,[57] N. Feege,[57] D. E. Fields,[44] M. Finger,[9] M. Finger, Jr.,[9] S. L. Fokin,[33]
J. E. Frantz,[46] A. Franz,[7] A. D. Frawley,[20] Y. Fukuda,[60] C. Gal,[57] P. Gallus,[15] P. Garg,[3,57] H. Ge,[57] F. Giordano,[25] A. Glenn,[35]
Y. Goto,[51,52] N. Grau,[2] S. V. Greene,[61] M. Grosse Perdekamp,[25] T. Gunji,[12] H. Guragain,[21] T. Hachiya,[51,52] J. S. Haggerty,[7]
K. I. Hahn,[19] H. Hamagaki,[12] H. F. Hamilton,[1] S. Y. Han,[19] J. Hanks,[57] S. Hasegawa,[29] T. O. S. Haseler,[21] K. Hashimoto,[51,53]
X. He,[21] T. K. Hemmick,[57] J. C. Hill,[28] K. Hill,[13] R. S. Hollis,[8] K. Homma,[22] B. Hong,[32] T. Hoshino,[22] N. Hotvedt,[28]
J. Huang,[7] S. Huang,[61] K. Imai,[29] J. Imrek,[16] M. Inaba,[60] A. Iordanova,[8] D. Isenhower,[1] Y. Ito,[42] D. Ivanishchev,[50]
B. V. Jacak,[57] M. Jezghani,[21] Z. Ji,[57] J. Jia,[7,56] X. Jiang,[36] B. M. Johnson,[7,21] V. Jorjadze,[57] D. Jouan,[48] D. S. Jumper,[25]
S. Kanda,[12] J. H. Kang,[64] D. Kapukchyan,[8] S. Karthas,[57] D. Kawall,[39] A. V. Kazantsev,[33] J. A. Key,[44] V. Khachatryan,[57]
A. Khanzadeev,[50] C. Kim,[8,32] D. J. Kim,[30] E.-J. Kim,[10] G. W. Kim,[19] M. Kim,[32,55] M. L. Kimball,[1] B. Kimelman,[41]
D. Kincses,[17] E. Kistenev,[7] R. Kitamura,[12] J. Klatsky,[20] D. Kleinjan,[8] P. Kline,[57] T. Koblesky,[13] B. Komkov,[50] J. R. Kotler,[41]
D. Kotov,[50,54] S. Kudo,[60] K. Kurita,[53] M. Kurosawa,[51,52] Y. Kwon,[64] R. Lacey,[56] J. G. Lajoie,[28] E. O. Lallow,[41] A. Lebedev,[28]
S. Lee,[64] S. H. Lee,[57] M. J. Leitch,[36] Y. H. Leung,[57] N. A. Lewis,[40] X. Li,[11] X. Li,[36] S. H. Lim,[36,64] L. D. Liu,[49] M. X. Liu,[36]
V-R Loggins,[25] V.-R. Loggins,[25] K. Lovasz,[16] D. Lynch,[7] T. Majoros,[16] Y. I. Makdisi,[6] M. Makek,[65] M. Malaev,[50] A. Manion,[57]
V. I. Manko,[33] E. Mannel,[7] H. Masuda,[53] M. McCumber,[36] P. L. McGaughey,[36] D. McGlinchey,[13] C. McKinney,[25] A. Meles,[45]
A. R. Mendez,[41] M. Mendoza,[8] A. C. Mignerey,[38] D. E. Mihalik,[57] A. Milov,[62] D. K. Mishra,[4] J. T. Mitchell,[7] G. Mitsuka,[52]
S. Miyasaka,[51,59] S. Mizuno,[51,60] A. K. Mohanty,[4] P. Montuenga,[25] T. Moon,[64] D. P. Morrison,[7] S. I. M. Morrow,[61]
T. V. Moukhanova,[33] T. Murakami,[34,51] J. Murata,[51,53] A. Mwai,[56] K. Nagai,[59] K. Nagashima,[22] T. Nagashima,[53] J. L. Nagle,[13]
M. I. Nagy,[17] I. Nakagawa,[51,52] H. Nakagomi,[51,60] K. Nakano,[51,59] C. Nattrass,[58] P. K. Netrakanti,[4] T. Niida,[60] S. Nishimura,[12]
R. Nouicer,[7,52] T. Novák,[18,63] N. Novitzky,[30,57] R. Novotny,[15] A. S. Nyanin,[33] E. O'Brien,[7] C. A. Ogilvie,[28]
J. D. Orjuela Koop,[13] J. D. Osborn,[40] A. Oskarsson,[37] G. J. Ottino,[44] K. Ozawa,[31,60] R. Pak,[7] V. Pantuev,[26] V. Papavassiliou,[45]
J. S. Park,[55] S. Park,[51,55,57] S. F. Pate,[45] M. Patel,[28] J.-C. Peng,[25] W. Peng,[61] D. V. Perepelitsa,[7,13] G. D. N. Perera,[45]
D. Yu. Peressounko,[33] C. E. PerezLara,[57] J. Perry,[28] R. Petti,[7,57] M. Phipps,[7,25] C. Pinkenburg,[7] R. Pinson,[1] R. P. Pisani,[7]
C. J. Press,[41] A. Pun,[46] M. L. Purschke,[7] J. Rak,[30] B. J. Ramson,[40] I. Ravinovich,[62] K. F. Read,[47,58] D. Reynolds,[56]
V. Riabov,[43,50] Y. Riabov,[50,54] D. Richford,[5] T. Rinn,[28] S. D. Rolnick,[8] M. Rosati,[28] Z. Rowan,[5] J. G. Rubin,[40] J. Runchey,[28]
A. S. Safonov,[54] B. Sahlmueller,[57] N. Saito,[31] T. Sakaguchi,[7] H. Sako,[29] V. Samsonov,[43,50] M. Sarsour,[21] K. Sato,[60] S. Sato,[29]
B. Schaefer,[61] B. K. Schmoll,[58] K. Sedgwick,[8] R. Seidl,[51,52] A. Sen,[28,58] R. Seto,[8] P. Sett,[4] A. Sexton,[38] D. Sharma,[57]
I. Shein,[24] T.-A. Shibata,[51,59] K. Shigaki,[22] M. Shimomura,[28,42] T. Shioya,[60] P. Shukla,[4] A. Sickles,[7,25] C. L. Silva,[36]
J. A. Silva,[41] D. Silvermyr,[37,47] B. K. Singh,[3] C. P. Singh,[3] V. Singh,[3] M. Slunečka,[9] K. L. Smith,[20] M. Snowball,[36]
R. A. Soltz,[35] W. E. Sondheim,[36] S. P. Sorensen,[58] I. V. Sourikova,[7] P. W. Stankus,[47] M. Stepanov,[39,†] H. Stien,[1] S. P. Stoll,[7]
T. Sugitate,[22] A. Sukhanov,[7] T. Sumita,[51] J. Sun,[57] S. Syed,[21] J. Sziklai,[63] A. Takeda,[42] A. Taketani,[51,52] K. Tanida,[29,52,55]
M. J. Tannenbaum,[7] S. Tarafdar,[61,62] A. Taranenko,[43,56] G. Tarnai,[16] R. Tieulent,[21] A. Timilsina,[28] T. Todoroki,[51,60]
M. Tomášek,[15] C. L. Towell,[1] R. Towell,[1] R. S. Towell,[1] I. Tserruya,[62] Y. Ueda,[22] B. Ujvari,[16] H. W. van Hecke,[36]
S. Vazquez-Carson,[13] J. Velkovska,[61] M. Virius,[15] V. Vrba,[15,27] N. Vukman,[65] X. R. Wang,[45,52] Z. Wang,[5] Y. Watanabe,[51,52]
Y. S. Watanabe,[12,31] F. Wei,[45] A. S. White,[40] C. P. Wong,[21] C. L. Woody,[7] M. Wysocki,[47] B. Xia,[46] C. Xu,[45] Q. Xu,[61] L. Xue,[21]
S. Yalcin,[57] Y. L. Yamaguchi,[12,52,57] H. Yamamoto,[60] A. Yanovich,[24] P. Yin,[13] J. H. Yoo,[32] I. Yoon,[55] H. Yu,[45,49]
I. E. Yushmanov,[33] W. A. Zajc,[14] A. Zelenski,[6] S. Zharko,[54] S. Zhou,[11] and L. Zou[8]

(PHENIX Collaboration)

[1]*Abilene Christian University, Abilene, Texas 79699, USA*
[2]*Department of Physics, Augustana University, Sioux Falls, South Dakota 57197, USA*
[3]*Department of Physics, Banaras Hindu University, Varanasi 221005, India*
[4]*Bhabha Atomic Research Centre, Bombay 400085, India*
[5]*Baruch College, City University of New York, New York, New York, 10010 USA*
[6]*Collider-Accelerator Department, Brookhaven National Laboratory, Upton, New York 11973-5000, USA*
[7]*Physics Department, Brookhaven National Laboratory, Upton, New York 11973-5000, USA*
[8]*University of California–Riverside, Riverside, California 92521, USA*
[9]*Charles University, Ovocný trh 5, Praha 1, 116 36, Prague, Czech Republic*
[10]*Chonbuk National University, Jeonju, 561-756, Korea*

[11]*Science and Technology on Nuclear Data Laboratory, China Institute of Atomic Energy,*
Beijing 102413, People's Republic of China
[12]*Center for Nuclear Study, Graduate School of Science, University of Tokyo, 7-3-1 Hongo,*
Bunkyo, Tokyo 113-0033, Japan
[13]*University of Colorado, Boulder, Colorado 80309, USA*
[14]*Columbia University, New York, New York 10027, and Nevis Laboratories, Irvington, New York 10533, USA*
[15]*Czech Technical University, Zikova 4, 166 36 Prague 6, Czech Republic*
[16]*Debrecen University, H-4010 Debrecen, Egyetem tér 1, Hungary*
[17]*ELTE, Eötvös Loránd University, H-1117 Budapest, Pázmány P. s. 1/A, Hungary*
[18]*Eszterházy Károly University, Károly Róbert Campus, H-3200 Gyöngyös, Mátrai út 36, Hungary*
[19]*Ewha Womans University, Seoul 120-750, Korea*
[20]*Florida State University, Tallahassee, Florida 32306, USA*
[21]*Georgia State University, Atlanta, Georgia 30303, USA*
[22]*Hiroshima University, Kagamiyama, Higashi-Hiroshima 739-8526, Japan*
[23]*Department of Physics and Astronomy, Howard University, Washington, D.C. 20059, USA*
[24]*IHEP Protvino, State Research Center of Russian Federation, Institute for High Energy Physics,*
Protvino 142281, Russia
[25]*University of Illinois at Urbana–Champaign, Urbana, Illinois 61801, USA*
[26]*Institute for Nuclear Research of the Russian Academy of Sciences, prospekt 60-letiya Oktyabrya 7a,*
Moscow 117312, Russia
[27]*Institute of Physics, Academy of Sciences of the Czech Republic, Na Slovance 2,*
182 21 Prague 8, Czech Republic
[28]*Iowa State University, Ames, Iowa 50011, USA*
[29]*Advanced Science Research Center, Japan Atomic Energy Agency, 2-4 Shirakata Shirane, Tokai-mura,*
Naka-gun, Ibaraki-ken 319-1195, Japan
[30]*Helsinki Institute of Physics and University of Jyväskylä, P.O. Box 35, FI-40014 Jyväskylä, Finland*
[31]*KEK, High Energy Accelerator Research Organization, Tsukuba, Ibaraki 305-0801, Japan*
[32]*Korea University, Seoul, 136-701, Korea*
[33]*National Research Center "Kurchatov Institute", Moscow, 123098 Russia*
[34]*Kyoto University, Kyoto 606-8502, Japan*
[35]*Lawrence Livermore National Laboratory, Livermore, California 94550, USA*
[36]*Los Alamos National Laboratory, Los Alamos, New Mexico 87545, USA*
[37]*Department of Physics, Lund University, Box 118, SE-22100 Lund, Sweden*
[38]*University of Maryland, College Park, Maryland 20742, USA*
[39]*Department of Physics, University of Massachusetts, Amherst, Massachusetts 01003-9337, USA*
[40]*Department of Physics, University of Michigan, Ann Arbor, Michigan 48109-1040, USA*
[41]*Muhlenberg College, Allentown, Pennsylvania 18104-5586, USA*
[42]*Nara Women's University, Kita-uoya Nishi-machi Nara 630-8506, Japan*
[43]*National Research Nuclear University, MEPhI, Moscow Engineering Physics Institute, Moscow, 115409, Russia*
[44]*University of New Mexico, Albuquerque, New Mexico 87131, USA*
[45]*New Mexico State University, Las Cruces, New Mexico 88003, USA*
[46]*Department of Physics and Astronomy, Ohio University, Athens, Ohio 45701, USA*
[47]*Oak Ridge National Laboratory, Oak Ridge, Tennessee 37831, USA*
[48]*IPN-Orsay, Université Paris-Sud, CNRS/IN2P3, Université Paris-Saclay, Boîte Postale, F-91406 Orsay, France*
[49]*Peking University, Beijing 100871, People's Republic of China*
[50]*PNPI, Petersburg Nuclear Physics Institute, Gatchina, Leningrad Region, 188300, Russia*
[51]*RIKEN Nishina Center for Accelerator-Based Science, Wako, Saitama 351-0198, Japan*
[52]*RIKEN BNL Research Center, Brookhaven National Laboratory, Upton, New York 11973-5000, USA*
[53]*Physics Department, Rikkyo University, 3-34-1 Nishi-Ikebukuro, Toshima, Tokyo 171-8501, Japan*
[54]*Saint Petersburg State Polytechnic University, Saint Petersburg 195251, Russia*
[55]*Department of Physics and Astronomy, Seoul National University, Seoul 151-742, Korea*
[56]*Chemistry Department, Stony Brook University, SUNY, Stony Brook, New York 11794-3400, USA*
[57]*Department of Physics and Astronomy, Stony Brook University, SUNY, Stony Brook, New York 11794-3800, USA*
[58]*University of Tennessee, Knoxville, Tennessee 37996, USA*
[59]*Department of Physics, Tokyo Institute of Technology, Oh-okayama, Meguro, Tokyo 152-8551, Japan*
[60]*Center for Integrated Research in Fundamental Science and Engineering, University of Tsukuba,*
Tsukuba, Ibaraki 305, Japan
[61]*Vanderbilt University, Nashville, Tennessee 37235, USA*
[62]*Weizmann Institute, Rehovot 76100, Israel*

^{63}*Institute for Particle and Nuclear Physics, Wigner Research Centre for Physics,*
Hungarian Academy of Sciences (Wigner RCP, RMKI), H-1525 Budapest 114, P.O. Box 49, Budapest, Hungary
^{64}*Yonsei University, IPAP, Seoul 120-749, Korea*
^{65}*University of Zagreb, Faculty of Science, Department of Physics, Bijenička 32, HR-10002 Zagreb, Croatia*
(Received 23 September 2016; published 9 March 2017)

The PHENIX Collaboration has measured the ratio of the yields of $\psi(2S)$ to $\psi(1S)$ mesons produced in $p + p$, $p +$ Al, $p +$ Au, and ^{3}He +Au collisions at $\sqrt{s_{NN}} = 200$ GeV over the forward and backward rapidity intervals $1.2 < |y| < 2.2$. We find that the ratio in $p + p$ collisions is consistent with measurements at other collision energies. In collisions with nuclei, we find that in the forward (p-going or ^{3}He-going) direction, the relative yield of $\psi(2S)$ mesons to $\psi(1S)$ mesons is consistent with the value measured in $p + p$ collisions. However, in the backward (nucleus-going) direction, the $\psi(2S)$ meson is preferentially suppressed by a factor of $\sim$2. This suppression is attributed in some models to the breakup of the weakly bound $\psi(2S)$ meson through final-state interactions with comoving particles, which have a higher density in the nucleus-going direction. These breakup effects may compete with color screening in a deconfined quark-gluon plasma to produce sequential suppression of excited quarkonia states.

I. INTRODUCTION

The production of quark-antiquark bound states in nuclear collisions has long been studied for evidence of a phase transition between normal nuclear matter, where quarks and gluons are confined in hadrons, to a plasma phase where colored partons are deconfined. Early predictions of charmonium suppression as an unambiguous signature of deconfinement [1] have proven to be overly simplistic, as a variety of competing mechanisms have been identified that do not require color screening to disrupt bound-state $q\bar{q}$ pair formation and hadronization. It is necessary to quantitatively account for these effects to correctly interpret what measurements of quarkonia suppression in nuclear collisions imply about the quantum-chromodynamics phase diagram.

The heavy charm and bottom quarks are of particular interest, because they are produced through hard processes that are calculable with perturbative quantum-chromodynamics techniques [2] and their bound states are accessible experimentally through decays to dileptons. Models of $c\bar{c}$ and $b\bar{b}$ bound-state production generally factorize quarkonia production into two stages: first, the prompt initial heavy-quark production via gluon fusion, and after a formation time τ_f, the mechanism leading to hadronization into the final color singlet state [3–5]. In collisions involving nuclei, the initial heavy-quark production can be affected by modifications of the parton distribution functions [6], energy loss in the nucleus [7], and scattering with other partons [8]. Effects which may be of hydrodynamic origin are also present in small systems [9–11] and may further alter the heavy-quark final state [12,13]. If these flow effects are due to quark-gluon-plasma formation, the presence of deconfined colored partons can inhibit coalescence into a bound state or dissolve fully formed bound states [14]. The fully formed pair may also be broken up through interactions with comoving hadrons outside the nucleus [15,16].

One way to isolate final-state effects is through studies of states with the same quark content but different binding energies, such as the charmonium states $\psi(1S)$ and $\psi(2S)$, with binding energies of $\sim$640 and $\sim$50 MeV, respectively [17]. Before the charmonium formation time $\tau_f \sim 0.15$ fm/c, the precursor state is thought to be the same and so any effects on the precursor are likely identical. While significant initial-state effects on open charm have been found at the Brookhaven National Laboratory (BNL) Relativistic Heavy Ion Collider (RHIC) [18,19], these should equally affect all charm pairs before projection onto a final state. Therefore any differences in the modification of $\psi(2S)$ and $\psi(1S)$ production are likely due to late time effects, which are sensitive to differences in the fully formed meson radius and binding energy.

Previous measurements of $\psi(2S)$ suppression in $p + A$ collisions by the E866/NuSea [20] and NA50 [21] experiments were found to be well explained by models based on the breakup of fully formed charmonium states inside the nucleus, which naturally leads to a larger effect on the $\psi(2S)$ due to its larger radius [22]. However, this model fails to reproduce data from $d +$ Au collisions at midrapidity at RHIC [23], where the higher beam energy and shorter nuclear crossing time mean the $c\bar{c}$ pairs project onto their final states outside the nucleus [24]. Breakup mechanisms that occur after the formation time can however explain the different suppression. Measurements over different rapidity intervals in asymmetric collisions can simultaneously provide information on the evolution of the $c\bar{c}$ state in different hadronic environments. In the $p/d/^3$He-going direction, there are relatively few produced particles, while in the A-going direction, there may be significant final-state interactions between the quarkonia state and the higher number of comoving hadrons.

Here, we present measurements of the relative yields of $\psi(2S)$ to $\psi(1S)$ mesons at forward and backward rapidity in $p + p$, $p +$ Al, $p +$ Au, and ^{3}He +Au collisions at $\sqrt{s_{NN}} = 200$ GeV, from the 2014 and 2015 PHENIX data sets. We find that the relative production rate of $\psi(2S)$ to $\psi(1S)$ mesons in $p + p$ collisions is consistent with expectations from a modified color evaporation model of charmonium

————————
*PHENIX spokesperson: akiba@rcf.rhic.bnl.gov
†Deceased.

production [25]. In $p/^3$He $+A$ collisions, over the forward ($p/^3$He-going) rapidity interval $1.2 < y < 2.2$ the relative production rates of the two states are consistent with what is found in $p + p$ collisions. However, over the backward (A-going) rapidity interval $-2.2 < y < -1.2$, the $\psi(2S)$ meson is preferentially more suppressed than the $\psi(1S)$ meson by a factor of ~ 2, which is likely due to final-state effects such as interactions with comoving hadrons.

II. EXPERIMENTAL SETUP

Dimuons from $\psi(2S)$ and $\psi(1S)$ decays were measured with the PHENIX muon spectrometer, which comprises two arms covering the forward and backward rapidity intervals $1.2 < |y| < 2.2$ [26]. Muons considered in this analysis pass through a forward vertex tracking detector (FVTX) [27], a hadron absorber with a thickness of ~ 10 interaction lengths, and then through three multiplane cathode strip tracking chambers that reside in a radial magnetic field. After the tracking chambers are more layers of absorbers and Iarocci tubes for muon identification, where tracks must penetrate at least 2.5 interaction lengths of additional steel absorber. The dimuon trigger used in this analysis records events that have two tracks in the same spectrometer arm that pass through all the absorber material.

Previous PHENIX measurements were not able to resolve the smaller $\psi(2S)$ peak in the dimuon mass spectrum near the larger, broad $\psi(1S)$ peak (cf. Refs. [28,29]). However, the introduction of the four silicon tracking layers of the FVTX in 2012 now allows a precise measurement of the pair opening angle to be made before the muons undergo multiple scattering in the absorber. The additional FVTX tracking improves the dimuon mass resolution and reduces combinatorial background from hadron decays, allowing separation of the two peaks.

III. DATA ANALYSIS

The measured dimuon mass spectra from $p + p$, $p + $ Al, $p + $ Au, and ^{3}He $+$ Au collisions at $\sqrt{s_{NN}} = 200$ GeV are shown in Fig. 1, with panels (a)–(d) [panels (e)–(h)] showing data recorded in the South (North) PHENIX muon spectrometer arm. These distributions are composed of peaks at the $\psi(1S)$ and $\psi(2S)$ masses (~ 3.1 and ~ 3.7 GeV/c^2, respectively) on top of correlated background from charm and bottom hadron decays and Drell-Yan pairs, plus combinatorial background from light meson decays and hadrons that are not stopped in the absorbers. The fits to the data are shown as a solid (black) line with a shaded (gray) band representing the 90% confidence level of the fit, with the resonances and total background components of the fit represented by dashed (blue) and dotted (red) lines, respectively.

The combinatorial background contribution is extracted using event mixing techniques and is normalized to match the like-sign background. To determine systematic uncertainties on the relative yields that vary from 1% in $p + p$ collisions to 4% in ^{3}He $+$ Au collisions, the mass range over which the normalization is done is varied from a nominal range of 2–5 GeV/c^2 to 1.5–5 and 2.5–5.5 GeV/c^2. The correlated

background is modeled in the fit by an exponential. In the fitting procedure, the combinatorial background contribution is fixed using the methods previously described, while the shape and normalization parameters of the correlated background are allowed to vary.

The resonances are represented in the fit by the sum of a crystal-ball function [30] plus a Gaussian. The crystal ball is a continuous piecewise function that is composed of a Gaussian on the high-mass side and an exponential on the low-mass side, which accounts for tails due to muon energy loss straggling in the absorbers. Due to 10 cm of additional steel absorber in the North arm as compared to the South arm, and the variations in the meson p_T spectra in the different collision systems, the low-mass tail on both peaks is expected to be different between the two arms and various systems. Therefore the parameters describing this low-side tail are allowed to float during fitting. The additional Gaussian is needed to account for tracks that have fewer than 14 hits out of a possible 16 in the muon tracker and therefore form pairs with poorer mass resolution. By analyzing pairs formed with one and two of these poorly reconstructed tracks, the width of the $\psi(1S)$ peak is found to vary from ~ 200 to ~ 250 MeV/c^2. Therefore, the width of this second Gaussian under the $\psi(1S)$ peak is set to 200 MeV/c^2 and varied by $\pm 25\%$ to determine a systematic uncertainty on the relative yields. From previous measurements and simulations [31], the width of the $\psi(2S)$ peak is expected to be 1.15 times the width of the $\psi(1S)$ peak; therefore the second Gaussian under this resonance is set to a nominal value of 230 MeV/c^2 and also varied by $\pm 25\%$. This is the dominant source of systematic uncertainty on this measurement, and it ranges from 8% in $p + p$ collisions to 37% in the Au-going direction in ^{3}He $+$ Au collisions, due to the larger combinatorial background.

The difference between the centers of the $\psi(2S)$ and $\psi(1S)$ peaks is set to the Particle Data Group value [32] of 0.589 MeV/c^2, and the width of the $\psi(2S)$ crystal-ball function is set to 1.15 times the width of the $\psi(1S)$ peak, again following expectations of the mass resolution in the muon spectrometer. This constraint is varied from 1.1 to 1.2 times the $\psi(1S)$ width to determine a systematic uncertainty on the relative yields of $\sim 3\%$ for all systems (variations outside this range do not converge on stable fit parameter values). Table I gives a summary of the counts measured in each collision system.

The physics quantity of interest here is the ratio of of the cross sections σ of the $\psi(2S)$ to $\psi(1S)$ mesons, multiplied by their respective branching ratio to dimuons, $B_{\mu\mu}$. The counts N_{meas} of each meson are determined by the fits to the dimuon mass spectra and are corrected for the PHENIX muon spectrometer pair acceptance Ω, the pair detection efficiency ϵ, and the dimuon trigger efficiency ϵ^{trig} for each species. The ratio of $\psi(2S)$ to $\psi(1S)$ mesons is given by

$$\frac{B_{\mu\mu}^{\psi(2S)}\sigma_{\psi(2S)}}{B_{\mu\mu}^{\psi(1S)}\sigma_{\psi(1S)}} = \frac{N_{\text{meas}}^{\psi(2S)}}{N_{\text{meas}}^{\psi(1S)}} \frac{\Omega_{\psi(1S)}\epsilon_{\psi(1S)}}{\Omega_{\psi(2S)}\epsilon_{\psi(2S)}} \frac{\epsilon_{\psi(1S)}^{\text{trig}}}{\epsilon_{\psi(2S)}^{\text{trig}}}. \quad (1)$$

The acceptance $\times$ efficiency factor $\frac{\Omega_{\psi(1S)}\epsilon_{\psi(1S)}}{\Omega_{\psi(2S)}\epsilon_{\psi(2S)}}$ is determined via a full GEANT4 simulation of the PHENIX detector [33]. A set of simulated dimuons, with a continuum of realistic mass,
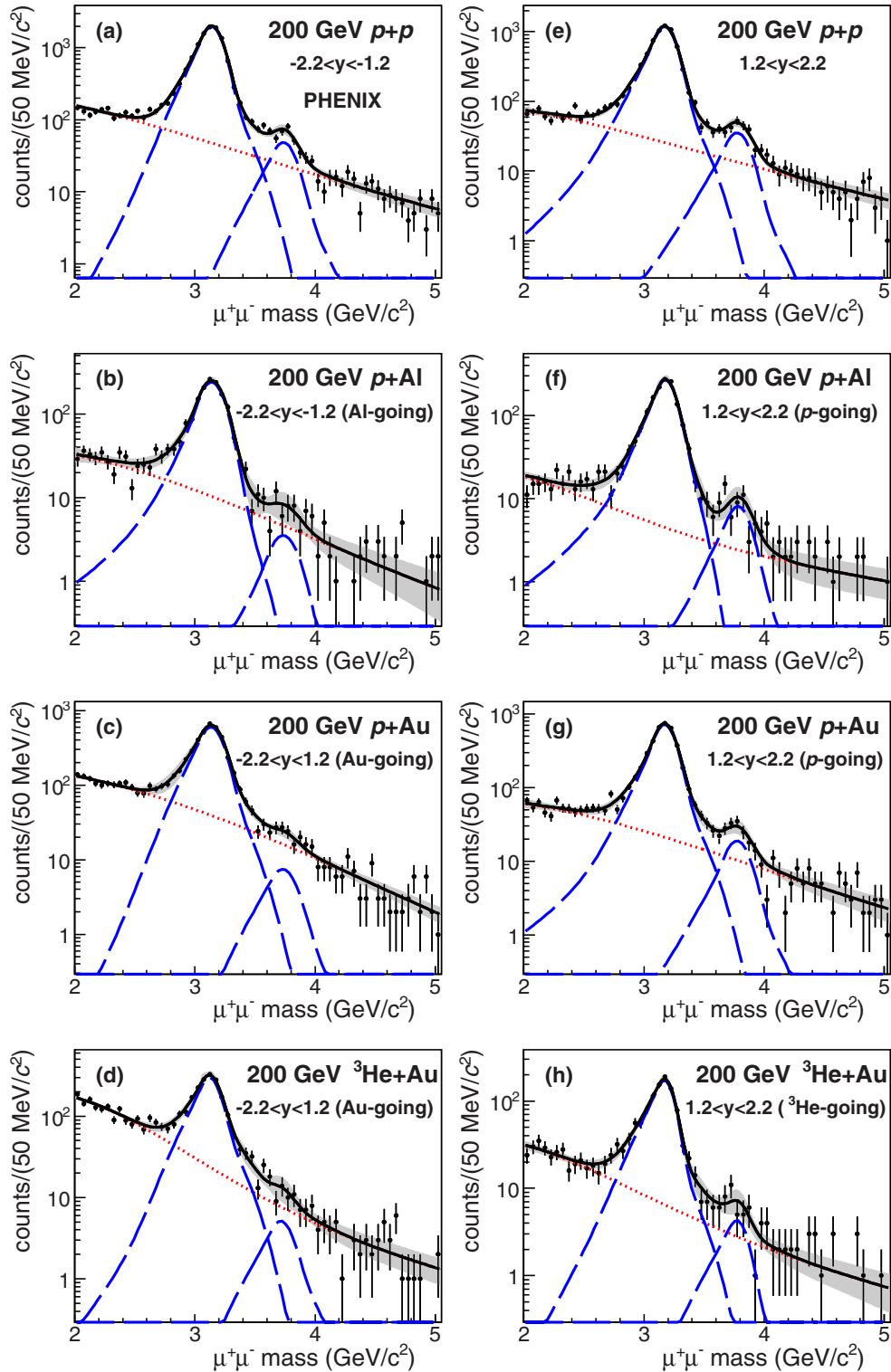
FIG. 1. The measured dimuon mass spectra with fits from the (a)–(d) South and (e)–(h) North PHENIX muon arms, for $p + p$, $p +$ Al, $p +$ Au, and ^{3}He +Au collisions at $\sqrt{s_{NN}} = 200$ GeV. The total fit is the solid (black) line with a shaded (gray) band representing the 90% confidence level. The dashed (blue) and dotted (red) lines represent the contributions from the resonances and the background, respectively.

p_T, and rapidity distributions, is passed through the simulated PHENIX detector. The ratio of the acceptance × efficiency at the $\psi(1S)$ mass value to the $\psi(2S)$ mass value is found to be ∼0.8 for each arm. Because the p_T distributions of $\psi(2S)$ and

$\psi(1S)$ mesons have not been measured in all the collision systems presented here, a systematic uncertainty on the acceptance × efficiency factor is determined by changing the assumed p_T spectra. Different dimuon samples are prepared

TABLE I. Summary of the measured ratios of $\psi(2S)/\psi(1S)$ mesons. The first (second) values in the rightmost column represent statistical (systematic) uncertainties.

Collision system	Rapidity interval	$N_{\text{meas}}^{\psi(1S)}$	$N_{\text{meas}}^{\psi(2S)}$	$\frac{B_{\mu\mu}^{\psi(2S)}\sigma_{\psi(2S)}}{B_{\mu\mu}^{\psi(1S)}\sigma_{\psi(1S)}}$ (%)
$p+p$	$1.2 < |y| < 2.2$	17120 ± 392	519 ± 51	$2.43 \pm 0.18 \pm 0.29$
$p+$Al	$1.2 < y < 2.2$ (p-going)	1497 ± 142	52 ± 11	$2.73 \pm 0.64 \pm 0.13$
$p+$Al	$-2.2 < y < -1.2$ (Al-going)	1463 ± 109	25 ± 11	$1.37 \pm 0.61 \pm 0.16$
$p+$Au	$1.2 < y < 2.2$ (p-going)	3893 ± 147	117 ± 18	$2.38 \pm 0.37 \pm 0.30$
$p+$Au	$-2.2 < y < -1.2$ (Au-going)	3561 ± 180	51 ± 18	$1.16 \pm 0.42 \pm 0.17$
^{3}He $+$Au	$1.2 < y < 2.2$ (^{3}He-going)	959 ± 64	27 ± 9.3	$2.24 \pm 0.78 \pm 0.32$
^{3}He $+$Au	$-2.2 < y < -1.2$ (Au-going)	1772 ± 132	35 ± 15	$1.59 \pm 0.67 \pm 0.60$

assuming the $\psi(1S)$ spectrum follows the distribution previously measured in $p + p$ collisions and $d +$ Au collisions at forward and backward rapidity [28] and m_T scaling [34] these distributions to approximate the $\psi(2S)$ spectrum. Adjusting the correction factors between these various assumptions gives a 2% systematic uncertainty on the relative yields.

The relative dimuon trigger efficiency $\epsilon_{\psi(1S)}^{\text{trig}}/\epsilon_{\psi(2S)}^{\text{trig}}$ is measured by finding the proportion of dimuon pairs in the minimum bias triggered data set that also fire the dimuon trigger. This small correction factor is $\sim$0.97, and a relative systematic uncertainty of 1% on the relative yields is assigned due to the statistical uncertainties on the dimuon sample in the minimum bias data set. Because no significant $\psi(1S)$ polarization has been measured at PHENIX [35], all corrections are calculated under the assumption that the mesons are unpolarized.

IV. RESULTS AND DISCUSSION

The p_T integrated ratios of $\psi(2S)$ to $\psi(1S)$ mesons extracted from the North and South spectrometer arms in the symmetric $p + p$ collision system agree within 2 standard deviations. These data points are averaged with a weighted least-squared procedure, using the inverse of the square of the statistical uncertainties as weights (the same procedure that is used by the Particle Data Group to combine measurements of the same quantity [32]). The resulting data point is shown in Fig. 2 and is consistent with world data taken at other collision energies. Little difference is observed in the ratio
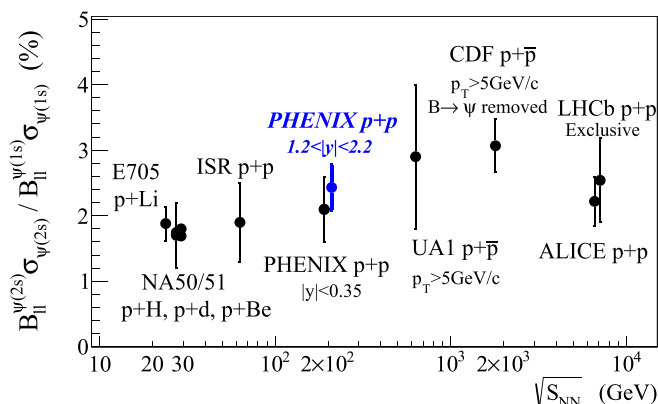
of $\psi(2S)$ to $\psi(1S)$ mesons produced in collisions with center-of-mass energies that range over nearly 3 orders of magnitude, within uncertainties. This may imply that despite significant differences in the total charm cross section across these energies, once a precursor $c\bar{c}$ is produced, the probability that it will project onto a given charmonium state is insensitive to the conditions that formed the initial $c\bar{c}$ pair.

The same ratio is shown as a function of p_T in Fig. 3, along with a calculation based on a modified color evaporation model of charmonium production at 200 GeV [25]. This model factorizes the initial production of the $c\bar{c}$ pair from the color neutralization process via emission of soft gluons. The ratios reported here are somewhat higher than the model for $p_T >$ 2 GeV/c, but the data's limited statistical precision and significant theoretical error bands preclude any firm conclusions.

From Fig. 1 it is apparent that the $\psi(2S)$ peaks are suppressed relative to the $\psi(1S)$ peak in the columns on the left (in the A-going direction). Quantitative comparisons are accomplished by calculating the double ratio of $\psi(2S)/\psi(1S)$ production in $p/^3$He $+A$ collisions to the ratio found in $p + p$ collisions, as shown in Fig. 4. A previously published data point from midrapidity $d +$ Au collisions at the same energy is also included for comparison [23]. We see that at forward rapidity, the double ratio is consistent with unity in all three collision systems, indicating that any possible nuclear effects on the two charmonium states are comparable. Because these

FIG. 2. Comparison of world data on the ratio of $\psi(2S)/\psi(1S)$ mesons in dilepton decays [21,29,36–42].
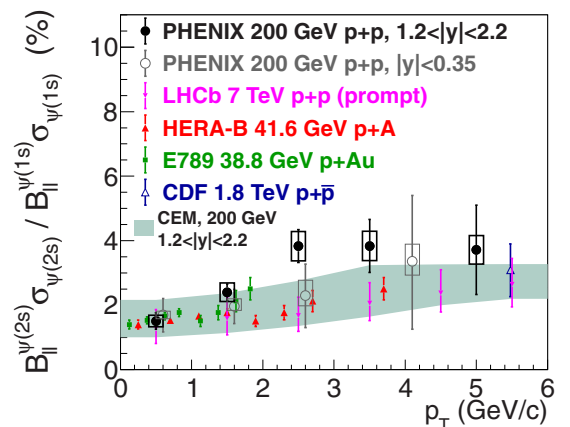

FIG. 3. Comparison of world data on the ratio of $\psi(2S)/\psi(1S)$ mesons as a function of p_T [29,40,43–45], along with a calculation from a color evaporation model (CEM) at $\sqrt{s} = 200$ GeV [25].
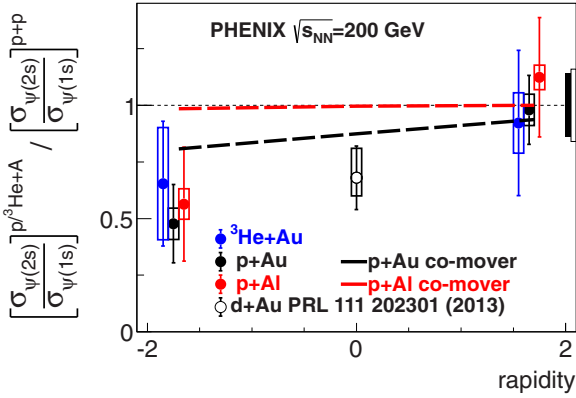
FIG. 4. The double ratio of $\psi(2S)/\psi(1S)$ mesons measured in $p/d/^3\mathrm{He}+A$ collisions to that same ratio in $p + p$ collisions at $\sqrt{s} = 200$ GeV, with a calculation based on breakup by comoving particles [47]. The bars (boxes) on the data points represent the statistical (systematic) uncertainties, and the shaded (open) box around unity represents the global uncertainty on the forward and backward (mid) rapidity data.

states are not fully formed until after they exit the nucleus, the fact that any nuclear effects have an equal magnitude on both states suggests that there are no significant final-state effects on the pair that occur in this rapidity region.

At backward rapidity, the ratios in all collision systems are suppressed by a factor of $\sim$2. The mechanism for this preferential suppression of the $\psi(2S)$ meson relative to the $\psi(1S)$ meson is expected to occur after the $\psi(1S)$ formation time. A significant difference in the late stages of the collision between this region and forward rapidity is the presence of a larger number of comoving hadrons (see Ref. [46] for measurements of the charged particle rapidity distributions in $d + \mathrm{Au}$, a similar collision system). Once the $c\bar{c}$ pair exits the nucleus, it may be subject to interactions with these particles that can lead to breakup of the charmonium state, which are expected to be more pronounced on the less tightly bound $\psi(2S)$ meson. While the exact nature of the interactions is not well understood, a model based on an absorption cross section that depends on the pair binding energy shows a preferential suppression that increases from forward to backward rapidity with comoving hadron multiplicity [47]. The model shows a similar trend with the $p + \mathrm{Au}$ data, although it underestimates the relative suppression at backward rapidity [see the solid (black) line in Fig. 4]. However, in $p + \mathrm{Al}$ collisions, the model predicts almost no relative suppression at backward rapidity [dotted (red) line], while the data show a relative suppression similar to that in $p + \mathrm{Au}$ collisions, within significant uncertainties.

Measurements in 5.02 TeV $p + \mathrm{Pb}$ collisions at the CERN Large Hadron Collider (LHC) have also shown that the $\psi(2S)$ meson is preferentially suppressed compared to the $\psi(1S)$ meson [48,49]. However, at this collision energy, the preferential suppression shows no significant rapidity dependence. This may indicate that the nuclear effects that preferentially suppress the $\psi(2S)$ meson are similar at forward and backward rapidity at the LHC. The charged-particle pseudorapidity density per participant nucleon $(dN_{\mathrm{ch}}/d\eta)/\langle N_{\mathrm{part}}\rangle$ in $p + \mathrm{Pb}$
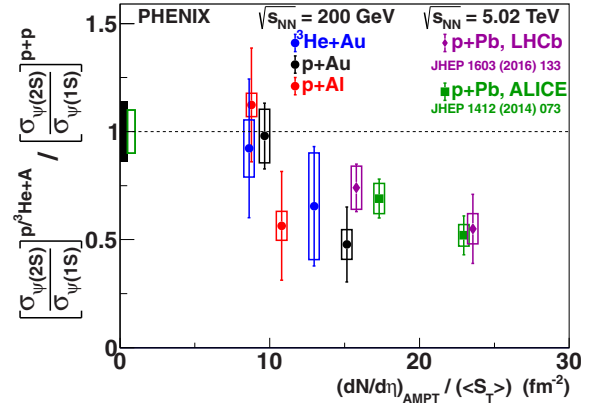

FIG. 5. The double ratio of $\psi(2S)/\psi(1S)$ mesons measured in $p/^3\mathrm{He}+A$ collisions to that same ratio in $p + p$ collisions as a function of comoving particle density. The shaded (black) [open (green)] box around unity represents the global uncertainty on the PHENIX (ALICE) data.

collisions at the LHC was found to be almost twice as high as that in $d + \mathrm{Au}$ collisions at RHIC [50], so interactions with comoving particles may be more significant, even at forward rapidity.

For a direct comparison, the double ratios measured by PHENIX and at the LHC are plotted together in Fig. 5 as a function of comoving particle density, which is defined as the particle multiplicity $dN/d\eta$ evaluated over the same rapidity interval as the charmonia measurement, divided by the nuclear overlap $\langle S_T\rangle$. Because measurements of the particle multiplicity do not exist for all these systems, the charged-particle multiplicity $dN_{\mathrm{ch}}/d\eta$ is determined by a multi-phase transport (AMPT) model simulations [51,52] and multiplied by $3/2$ to give the approximate total particle multiplicity $dN/d\eta$. The nuclear overlap $\langle S_T\rangle$ is defined as

$$\langle S_T\rangle = 4\pi\sqrt{\langle x^2\rangle\langle y^2\rangle - \langle xy\rangle^2}, \qquad (2)$$

where x and y are the spatial coordinates of the participating nucleons. This quantity is found via Monte Carlo Glauber simulations of the various collision species [53], with the $^3\mathrm{He}$ geometry modified as described in Ref. [54]. Table II summarizes the results of these simulations.

Figure 5 shows that the double ratio decreases as the comoving particle density increases, which is qualitatively consistent with expectations of charmonium breakup through final-state interactions. The forward-rapidity PHENIX data at relatively low comover density shows no preferential suppression of $\psi(2S)/\psi(1S)$, but the forward rapidity LHC data show a relative suppression that is comparable to the backward rapidity PHENIX data at similar comover density, within uncertainties. The backward LHC data, at the highest comover density, also shows relative suppression.

Understanding suppression due to comovers could play a critical role in interpreting quarkonia data from $A + A$ collisions. Existing data on excited charmonia states in $A + A$ collisions generally suffer from poor statistics and large combinatorial backgrounds and cover limited p_T ranges [55,56]. However, a clear sequential suppression of the excited

TABLE II. The charged-particle multiplicity $dN_{ch}/d\eta$ determined from AMPT simulations [51,52] and the nuclear overlap S_T from Glauber simulations [53,54] for the data shown in Fig. 5. Here we assume $dN/d\eta = \frac{3}{2}dN_{ch}/d\eta$ (see text).

Collision system	$\sqrt{s_{NN}}$	Rapidity interval	$(dN_{ch}/d\eta)_{AMPT}$	$\langle S_T \rangle$ (fm^2)	$\frac{(dN/d\eta)_{AMPT}}{\langle S_T \rangle}$ (fm^{-2})
p + Al	200 GeV	$-2.2 < y < -1.2$	5.9	0.82	10.8
p + Al	200 GeV	$1.2 < y < 2.2$	4.8	0.82	8.8
p + Au	200 GeV	$-2.2 < y < -1.2$	10.2	1.01	15.1
p + Au	200 GeV	$1.2 < y < 2.2$	6.5	1.01	9.7
^{3}He+Au	200 GeV	$-2.2 < y < -1.2$	20.3	2.35	13.0
^{3}He+Au	200 GeV	$1.2 < y < 2.2$	13.5	2.35	8.6
p + Pb	5.02 TeV	$-4.46 < y < -2.03$	19.9	1.3	23.0
p + Pb	5.02 TeV	$2.03 < y < 3.53$	15	1.3	17.3
p + Pb	5.02 TeV	$-4.0 < y < -2.5$	20.4	1.3	23.5
p + Pb	5.02 TeV	$2.5 < y < 4.0$	13.7	1.3	15.8

bottomonium states has been observed in Pb + Pb collisions at the LHC [57]. While color screening is expected to play a role, given the high charged-particle density in these collisions, it is reasonable to expect that similar breakup mechanisms can also have an effect on these states. In particular, the highly suppressed $\Upsilon(3S)$ state has a binding energy of only $\sim$200 MeV and may be especially sensitive to breakup through interactions with comoving particles.

V. CONCLUSIONS

In conclusion, we have found that the relative production of $\psi(2S)$ to $\psi(1S)$ mesons in $p + p$ collisions at $\sqrt{s} = 200$ GeV is consistent with expectations from a modified color evaporation model of charmonium production. In $p/^3$He $+A$ collisions at forward rapidity we observe no difference in the $\psi(2S)/\psi(1S)$ ratio relative to $p + p$ collisions, which indicates that any possible nuclear effects that are present in this rapidity region are common between the two states and therefore appear to occur on a time scale that is short compared to the charmonium formation time. At backward rapidity, where the comoving particle density is higher, we find that the $\psi(2S)$ meson is preferentially suppressed by a factor of $\sim$2. This effect is likely not due to any interaction in the nucleus, because the $c\bar{c}$ pair exits the nucleus before final meson formation occurs. The preferential suppression appears consistent with interactions of the fully formed color-neutral meson with comoving particles. The magnitude of this breakup mechanism is dependent on the meson binding energy and is likely important for interpretation of the sequential screening of quarkonia in $A + A$ collisions.

[1] T. Matsui and H. Satz, J/ψ suppression by quark-gluon plasma formation, Phys. Lett. B **178**, 416 (1986).

[2] M. Cacciari, P. Nason, and R. Vogt, QCD Predictions for Charm and Bottom Production at RHIC, Phys. Rev. Lett. **95**, 122001 (2005).

[3] H. Fritzsch, Producing heavy quark flavors in hadronic collisions: A test of quantum chromodynamics, Phys. Lett. B **67**, 217 (1977).

[4] G. T. Bodwin, E. Braaten, and J. Lee, Comparison of the color-evaporation model and the NRQCD factorization

approach in charmonium production, Phys. Rev. D **72**, 014004 (2005).

[5] Z. B. Kang, Y. Q. Ma, J. W. Qiu, and G. Sterman, Heavy quarkonium production at collider energies: Factorization and evolution, Phys. Rev. D **90**, 034006 (2014).

[6] I. Helenius, K. J. Eskola, H. Honkanen, and C. A. Salgado, Impact-parameter dependent nuclear parton distribution functions: EPS09s and EKS98s and their applications in nuclear hard processes, J. High Energy Phys. 07 (2012) 073.

[7] I. Vitev, Non-Abelian energy loss in cold nuclear matter, Phys. Rev. C **75**, 064906 (2007).

[8] R. Vogt, The *A* dependence of open charm and bottom production, Int. J. Mod. Phys. E **12**, 211 (2003).

[9] A. Adare *et al.* (PHENIX Collaboration), Quadrupole Anisotropy in Dihadron Azimuthal Correlations in Central d + Au Collisions at $\sqrt{s_{NN}}$ = 200 GeV, Phys. Rev. Lett. **111**, 212301 (2013).

[10] A. Adare *et al.* (PHENIX Collaboration), Measurement of Long-Range Angular Correlation and Quadrupole Anisotropy of Pions and (Anti)protons in Central d + Au Collisions at $\sqrt{s_{NN}}$ = 200 GeV, Phys. Rev. Lett. **114**, 192301 (2015).

[11] A. Adare *et al.* (PHENIX Collaboration), Measurements of Elliptic and Triangular Flow in High-Multiplicity ^{3}He +Au Collisions at $\sqrt{s_{NN}}$ = 200 GeV, Phys. Rev. Lett. **115**, 142301 (2015).

[12] X. Du and R. Rapp, Sequential regeneration of charmonia in heavy-ion collisions, Nucl. Phys. A **943**, 147 (2015).

[13] A. Beraudo *et al.*, Heavy-flavour production in high-energy *d*-Au and *p*-Pb collisions, J. High Energy Phys. 03 (2016) 123.

[14] A. Mocsy, P. Petreczky, and M. Strickland, Quarkonia in the quark gluon plasma, Int. J. Mod. Phys. A **28**, 1340012 (2013).

[15] A. Capella, A. Kaidalov, A. Kouider Akil, and C. Gerschel, J/ψ and ψ' suppression in heavy ion collisions, Phys. Lett. B **393**, 431 (1997).

[16] E. G. Ferreiro, Excited charmonium suppression in proton-nucleus collisions as a consequence of comovers, Phys. Lett. B **749**, 98 (2015).

[17] H. Satz, Colour deconfinement and quarkonium binding, J. Phys. G **32**, R25 (2006).

[18] A. Adare *et al.* (PHENIX Collaboration), Cold-Nuclear-Matter Effects on Heavy-Quark Production in d + Au Collisions at $\sqrt{s_{NN}}$ = 200 GeV, Phys. Rev. Lett. **109**, 242301 (2012).

[19] A. Adare *et al.* (PHENIX Collaboration), Cold-Nuclear-Matter Effects on Heavy-Quark Production at Forward and Backward Rapidity in d + Au Collisions at $\sqrt{s_{NN}}$ = 200 GeV, Phys. Rev. Lett. **112**, 252301 (2014).

[20] M. J. Leitch *et al.* (NuSea Collaboration), Measurement of J/ψ and ψ' Suppression in *p*-A collisions at 800-GeV/*c*, Phys. Rev. Lett. **84**, 3256 (2000).

[21] B. Alessandro *et al.* (NA50 Collaboration), J/ψ and ψ' production and their normal nuclear absorption in proton-nucleus collisions at 400 GeV, Eur. Phys. J. C **48**, 329 (2006).

[22] F. Arleo, P. B. Gossiaux, T. Gousset, and J. Aichelin, Charmonium suppression in *pA* collisions, Phys. Rev. C **61**, 054906 (2000).

[23] A. Adare *et al.* (PHENIX Collaboration), Nuclear Modification of ψ', χ_c, and J/ψ Production in d + Au Collisions at $\sqrt{s_{NN}}$ = 200 GeV, Phys. Rev. Lett. **111**, 202301 (2013).

[24] D. C. McGlinchey, A. D. Frawley, and R. Vogt, Impact parameter dependence of the nuclear modification of J/ψ production in d + Au collisions at $\sqrt{s_{NN}}$ = 200 GeV, Phys. Rev. C **87**, 054910 (2013).

[25] Y. Q. Ma and R. Vogt (private communication and unpublished).

[26] H. Akikawa *et al.* (PHENIX Collaboration), PHENIX muon arms, Nucl. Instrum. Methods Phys. Res., Sect. A **499**, 537 (2003).

[27] C. Aidala *et al.*, The PHENIX forward silicon vertex detector, Nucl. Instrum. Methods Phys. Res., Sect. A **755**, 44 (2014).

[28] A. Adare *et al.* (PHENIX Collaboration), Transverse-momentum dependence of the J/ψ nuclear modification in d + Au collisions at $\sqrt{s_{NN}}$ = 200 GeV, Phys. Rev. C **87**, 034904 (2013).

[29] A. Adare *et al.* (PHENIX Collaboration), Ground and excited charmonium state production in p + p collisions at $\sqrt{s}$ = 200 GeV, Phys. Rev. D **85**, 092004 (2012).

[30] T. Skwarnicki, *A Study of the Radiative CASCADE Transitions between the Upsilon-Prime and Upsilon Resonances*, Ph.D. thesis (Cracow, INP, 1986).

[31] R. K. Choudhury *et al.*, Technical Design Report of the Forward Silicon Vertex Tracker, 2007.

[32] K. A. Olive *et al.* (Particle Data Group), Review of particle physics, Chin. Phys. C **38**, 090001 (2014).

[33] S. Agostinelli *et al.* (GEANT4 Collaboration), GEANT4: A simulation toolkit, Nucl. Instrum. Methods Phys. Res., Sect. A **506**, 250 (2003).

[34] A. Adare *et al.* (PHENIX Collaboration), Measurement of neutral mesons in p + p collisions at $\sqrt{(s)}$ = 200 GeV and scaling properties of hadron production, Phys. Rev. D **83**, 052004 (2011).

[35] A. Adare *et al.* (PHENIX Collaboration), Transverse momentum dependence of J/ψ polarization at midrapidity in p + p collisions at $\sqrt{s}$ = 200 GeV, Phys. Rev. D **82**, 012001 (2010).

[36] L. Antoniazzi *et al.* (E705 Collaboration), Production of J/ψ via ψ' and χ Decay in 300 GeV/*cp* and $\pi^\pm$ Nucleon Interactions, Phys. Rev. Lett. **70**, 383 (1993).

[37] M. C. Abreu *et al.* (NA51 Collaboration), J/ψ, ψ' and Drell-Yan production in p + p and p + d interactions at 450 GeV/*c*, Phys. Lett. B **438**, 35 (1998).

[38] A. G. Clark *et al.*, Electron pair production at the CERN ISR, Nucl. Phys. B **142**, 29 (1978).

[39] C. Albajar *et al.* (UA1 Collaboration), J/ψ and ψ' production at the CERN $p\bar{p}$ collider, Phys. Lett. B **256**, 112 (1991).

[40] F. Abe *et al.* (CDF Collaboration), J/ψ and $\psi(2S)$ Production in $p\bar{p}$ Collisions at $\sqrt{s}$ = 1.8 TeV, Phys. Rev. Lett. **79**, 572 (1997).

[41] R Aaij *et al.* (LHCb Collaboration), Exclusive J/ψ and $\psi(2S)$ production in pp collisions at $\sqrt{s}$ = 7 TeV, J. Phys. G **40**, 045001 (2013).

[42] B. B. Abelev *et al.* (ALICE Collaboration), Measurement of quarkonium production at forward rapidity in pp collisions at $\sqrt{s}$ = 7 TeV, Eur. Phys. J. C **74**, 2974 (2014).

[43] R Aaij *et al.* (LHCb Collaboration), Measurement of $\psi(2S)$ meson production in pp collisions at $\sqrt{s}$ = 7 TeV, Eur. Phys. J. C **72**, 2100 (2012).

[44] I. Abt *et al.* (HERA-B Collaboration), A measurement of the ψ' to J/ψ production ratio in 920 GeV proton-nucleus interactions, Eur. Phys. J. C **49**, 545 (2007).

[45] M. H. Schub *et al.* (E789 Collaboration), Measurement of J/ψ and ψ' production in 800 GeV/*c* proton-gold collisions, Phys. Rev. D **52**, 1307 (1995); **53**, 570E (1996).

[46] B. Alver *et al.* (PHOBOS Collaboration), Phobos results on charged particle multiplicity and pseudorapidity distributions in Au + Au, Cu + Cu, d + Au, and p + p collisions at ultra-relativistic energies, Phys. Rev. C **83**, 024913 (2011).

[47] E. G. Ferreiro (private communication).

[48] B. B. Abelev *et al.* (ALICE Collaboration), Suppression of $\psi(2S)$ production in p-Pb collisions at $\sqrt{s_{NN}} = 5.02$ TeV, J. High Energy Phys. 12 (2014) 073.

[49] R. Aaij *et al.* (LHCb Collaboration), Study of $\psi(2S)$ production and cold nuclear matter effects in p-Pb collisions at $\sqrt{s_{NN}} = 5$ TeV, J. High Energy Phys. 03 (2016) 133.

[50] B. Abelev *et al.* (ALICE Collaboration), Pseudorapidity Density of Charged Particles in p + Pb Collisions at $\sqrt{s_{NN}} = 5.02$ TeV, Phys. Rev. Lett. **110**, 032301 (2013).

[51] Z. W. Lin, C. M. Ko, and S. Pal, Partonic Effects on Pion Interferometry at RHIC, Phys. Rev. Lett. **89**, 152301 (2002).

[52] Z. W. Lin,, C. M. Ko, B. A. Li, B. Zhang, and S. Pal, Multiphase transport model for relativistic heavy ion collisions, Phys. Rev. C **72**, 064901 (2005).

[53] C. Loizides, J. Nagle, and P. Steinberg, Improved version of the PHOBOS Glauber Monte Carlo, Software X **1-2**, 13 (2015).

[54] J. L. Nagle, A. Adare, S. Beckman, T. Koblesky, J. O. Koop, D. McGlinchey, P. Romatschke, J. Carlson, J. E. Lynn, and M. McCumber, Exploiting Intrinsic Triangular Geometry in Relativistic ^{3}He +Au Collisions to Disentangle Medium Properties, Phys. Rev. Lett. **113**, 112301 (2014).

[55] J. Adam *et al.* (ALICE Collaboration), Differential studies of inclusive J/ψ and $\psi(2S)$ production at forward rapidity in Pb-Pb collisions at $\sqrt{s_{NN}} = 2.76$ TeV, J. High Energy Phys. 05 (2016) 179.

[56] V. Khachatryan *et al.* (CMS Collaboration), Measurement of Prompt $\psi(2S) \to J/\psi$ Yield Ratios in Pb-Pb and p-p Collisions at $\sqrt{s_{NN}} = 2.76$ TeV, Phys. Rev. Lett. **113**, 262301 (2014).

[57] S. Chatrchyan *et al.* (CMS Collaboration), Observation of Sequential Υ Suppression in PbPb Collisions, Phys. Rev. Lett. **109**, 222301 (2012).